Computer Simulations of Direct Imaging of Extrasolar Planets

Uday E. Jallod* and A.T. Mohammed
Department of Astronomy, College of Science, University of Baghdad, Baghdad-Iraq

Abstract

Numerical simulations are carried out to investigate the possibility of observing extrasolar planet nearby star via optical telescopes. Several techniques are considered in this study in order to quantitatively assess their quality in suppressing the wings of the point spread function of optical telescope of a reference star. The optical telescope with circular Gaussian shape aperture reveals extrasolar planet even with contrast ratio 10^{-7} while the square Gaussian shape aperture reveals the planet with 10^{-5}.

Keywords: Fourier optics, optical imaging systems, extrasolar planets.

محاكاة حاسوبية للتصوير المباشر للكواكب الخارجية

عدي عطيوي جلود و علي طالب محمد
قسم الفلك، كلية العلوم، جامعة بغداد، بغداد–العراق

الخلاصة

محاكاة عددية نفذت لتحقيق امكانية رصد كوكب قرب نجم معين بواسطة التلسكوبات البصرية. عدة تقنيات اختيرت في هذه الدراسة لكي تقيم وبصورة كمية كفائتها في خفض اطراف دالة الانتشار النقطية للنجم. اظهرت النتائج ان التلسكوب البصري ذو فتحة دائرية كاوسية الشكل تتحسس الكوكب عند نسبة تباين مقدارها 10^{-7} بينما بالنسبة للفتحة المربعة الكاوسية الشكل كانت $^{-5}$١٠.

*Email: udayjallod@yahoo.com

1. Introduction

High contrast imaging at a dynamic range of 10^{-9} to 10^{-10} of nearby stars has considered to be one of a valuable methods to detect extrasolar planets [1]. This is an important challenge of direct imaging of extresolar planet [2]. The planet is much fainter than the star and angularly very close, with a contrast of approximatily10^{-9} and angular separation of nearly 0.5" at about 10 Pc [3]. In the past few years, several techniques were implemented on moderate telescope such as (shape of pupil, obstructing aperture, Gaussian pupil, , ect.) to detect such planets [4].

An important criterion in creating high contrast imaging of a ground based optical telescope is to keep scattered light from the star to be as minimum as possible. Adaptive optics (AO) have been applied in astronomical instrumentation in order to give much higher spatial resolution and the high dynamic range allowing the environments of bright objects to be studied much closer than before [5].

Many coronograph concepts have been developed over the last ten years, most of them derived from Bernard Loyt orginal design (Lyot 1939) [6]. There are number of different techniques currently used to observe extrasolar planets, since the first report by Mayor & Queloz (1995) [7, 8, 9].

In order to observe extrasolar planet with ground based optical telescope, the apodization technique have been used to control the shape of the aperture telescope owing to suppress the diffraction-limited image of the star or restoring the diffraction-limited image of the extrsolar planet by reducing the peak power of the star relative to the reflected peak power of the planet [10].

2. Mathematical Formulation and Simulations

The design of the shaped pupil of optical telescope is a vital element for direct imaging of extrasolar planets around nearby stars, because it control the amount of suppressing the wings of the point spread function (psf) owing to reveal the planet that buried beneath the star [11]. The requirements of optical telescope have to be able to cancel starlight up to a 10^{10} factor and provide a good high angular resolution of psf [12].

The most basic aperture shape of the optical telescope is a circular aperture that having a constant transmission inside the pupil and zero outside the pupil according to the following equation [13].

$$P_c(\zeta, \gamma) = \begin{cases} 1 & \text{if } \rho \le R \\ 0 & \text{otherwise} \end{cases} \quad (1)$$

where R is the radius of the telescope and ρ is given by:

$$\rho = ((\zeta - \zeta_c)^2 + (\gamma - \gamma_c)^2)^{1/2} \quad (2)$$

(ζ_c, γ_c) is the center of a two-dimensional array. The intensity of the psf of a diffraction-limited telescope is just the square absolute value of the Fourier transform of the pupil function [14]. The psf is given by:

$$psf(x, y) = \left| FT(P_c(\zeta, \gamma)) \right|^2 \quad (3)$$

where FT denotes Fourier transform operator. figure 1 shows the results after implementing equations 1 & 3 using an array of size 256 by 256 pixels and R=60 pixels.

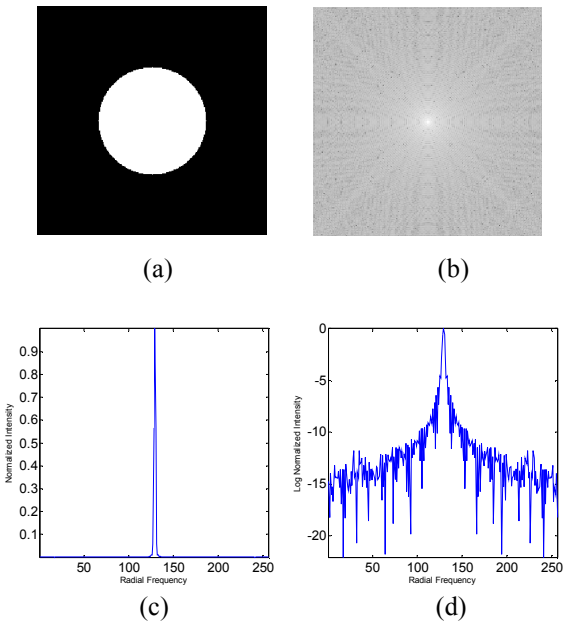

(a) (b) (c) (d)

Figure 1- (a) Circle aperture, (b) Logarithmic scale image of a normalized psf, (c) Central plot through a normalized psf, and (d) Central plot through (b).

The square aperture is given by [15]:

$$P_s(\zeta,\gamma) = \begin{cases} 1 & \text{if } -R< x <+R \ \& \ -R< y <+R \\ 0 & \text{otherwise} \end{cases} \quad (4)$$

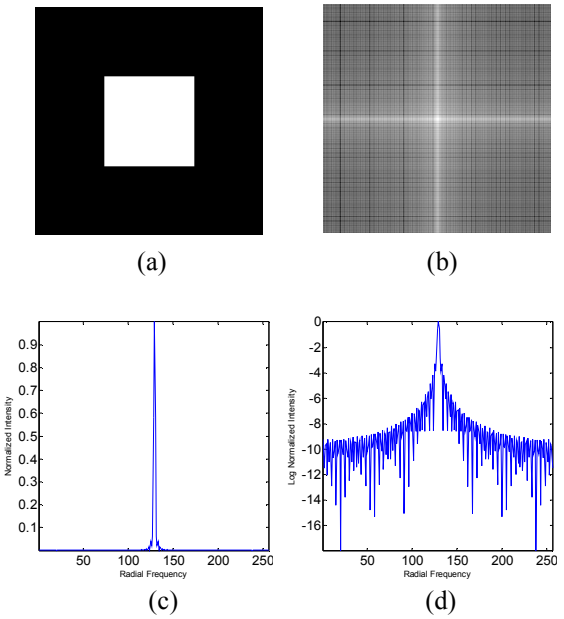

Figure 2- (a) Square aperture, (b) Logarithmic scale image of a normalized psf, (c) Central plot of a normalized psf, and (d) Central plot through (b).

The circular or square Gaussian shape aperture is given by [16]:

$$P_G(\zeta,\gamma) = \begin{cases} \exp\left(\frac{(\zeta-\rho)^2}{2\sigma^2}\right) & \text{inside } P_c \text{ or } P_s \\ 0 & \text{otherwise} \end{cases} \quad (5)$$

where σ is the standard deviation of a Gaussian function and considered to be an important parameter that control the width of the Gaussian function. The results of implementing equation 5 with different values of σ using circular aperture are demonstrated in figure 3.

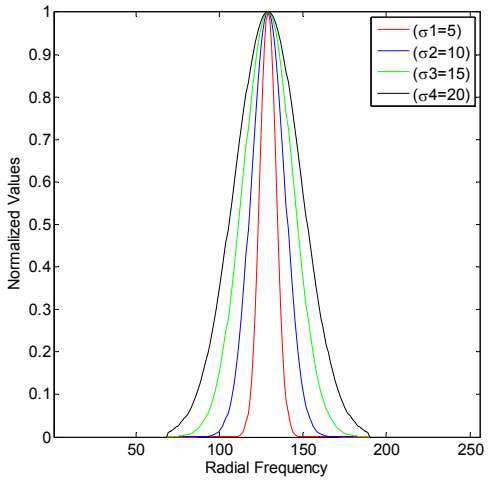

Figure 3- Central plot through a normalized circular Gaussian shape aperture at different values of σ.

The two-dimensional circular Gaussian shape aperture and the corresponding psf are computed and displayed in figure 4.

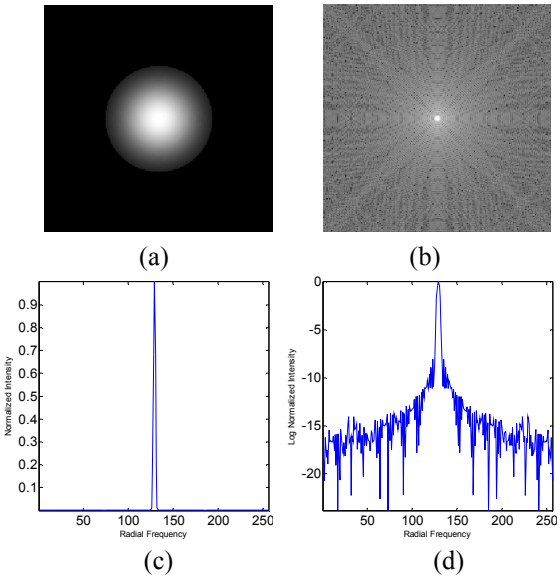

Figure 4- (a) Circular Gaussian shape aperture at σ =30, (b) Logarithmic image of a normalized psf, (c) Central plot through a normalized psf, and (d) Central plot through (b).

The results of implementing equation 5 with different values of σ using square aperture are demonstrated in figure 5 .

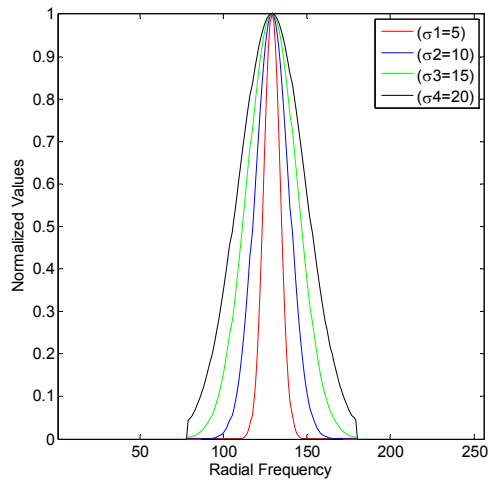

Figure 5- Central plot through a normalized square Gaussian shape aperture at different value of σ.

The two-dimensional square Gaussian shape aperture and its psf are demonstrated in figure 6.

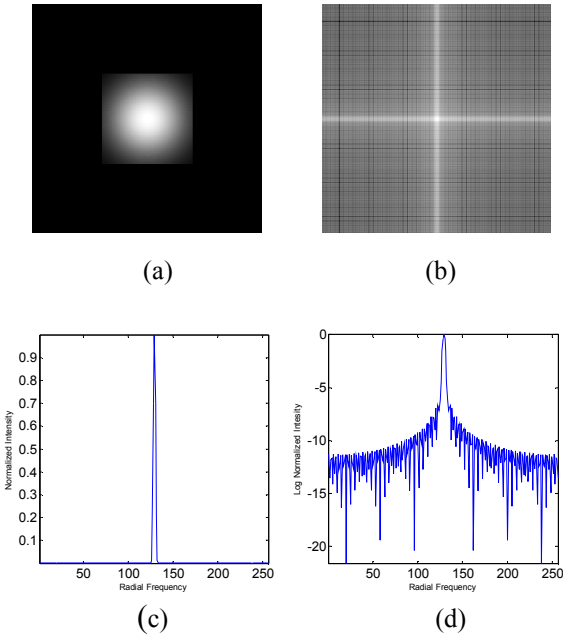

Figure 6- (a) Square Gaussian shape aperture at σ =30, (b) Logarithmic scale image of a normalized psf, (c) Central plot through a normalized psf, and (d) Central plot through (b).

It is of interest now to compare the results that obtained from these apertures. The logarithmic scales of the normalized psf with different shape apertures of equal radius are shown in figure 7.

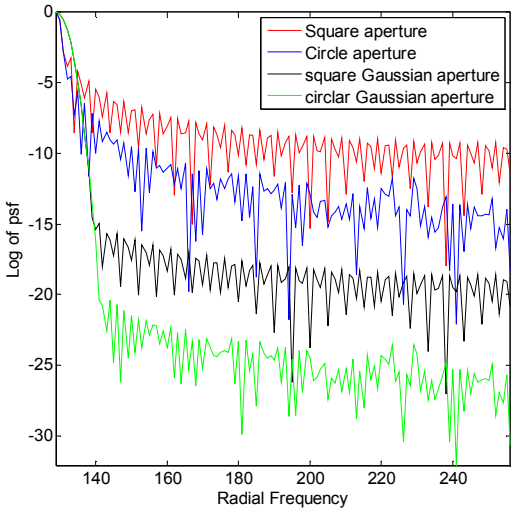

Figure 7- Central line through logarithmic scale of a normalized psf using different shape apertures.

It should be pointed out that the best value of σ for both circular and square Gaussian shape apertures was found to be 15.

σ of circular and square Gaussian shape apertures is a vital parameter that suppressing the high frequency components of the wings of the psf or star and this is a crucial point in observing extrasolar planet nearby star.

It is of importance to make a tradeoff between the minimum value of the logarithmic scale of a normalized psf that computed by a circular and a square Gaussian shape apertures and the distance of the psf when the first oscillation start to build up as we are moving away from the center of an array. figures 8 & 9 illustrate these details.

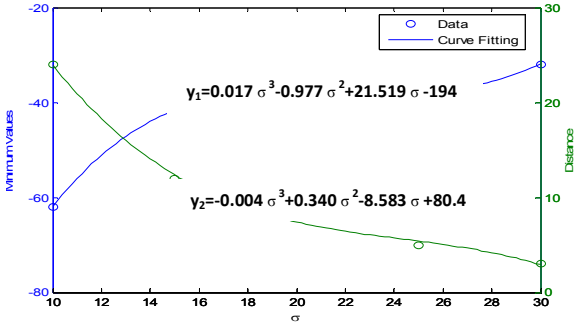

Figure 8- The relationship between minimum value and distance of the logarithmic scale of the normalized psf for a circular Gaussian shape aperture as a function of σ.

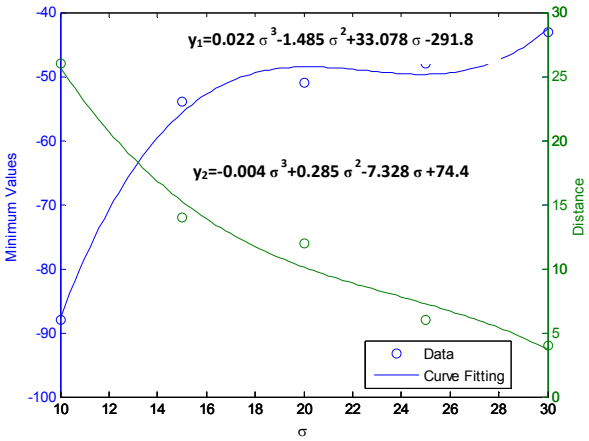

Figure 9- The relationship between minimum value and distance of the logarithmic scale of the normalized psf for a square Gaussian shape aperture as a function of σ.

y_1 & y_2 are the third degree polynomial equations that fitted the data demonstrated in above figures.

To assess the quality of these techniques in observing extrasolar planet by optical telescope, a binary system is generated as follows:

$$B(x,y) = A*e^{-((x-x_c)^2+(y-y_c+d)^2/(2*\sigma_2^2))} + e^{-((x-x_c)^2+(y-y_c-d)^2/(2*\sigma_2^2))} \quad (6)$$

where A is the brightness of the star while the reflected brightness of the planet kept constant at a value of one, so that, the contrast ratio (CR) is the ratio of the brightness of the planet to the brightness of the star. This is equivalent to (1/A) and d is the separation distance between star & planet. d is taken to be 10 pixels to ensure the planet lies beneath the wings of the radial frequency components of the psf of the optical telescope in use. σ_1 and σ_2 are the standard deviations of the star and the planet respectively and taken to be 3.

The image of the binary system that could be observed by optical telescope is the convolution between equation. 3 and equation. 6 are given by the following equation [17]:

$$C(x, y) = \iint_{-\infty}^{\infty} B(x',y')psf(x-x',y-y')dx'dy' \quad (7)$$

The above equation could also be written as:

$$C(x,y) = B(x, y) \otimes psf(x,y) \quad (8)$$

where $\otimes$ denotes convolution.

This equation demonstrates the observation of star and planet by optical telescope in the absence of atmospheric turbulence and any geometrical aberration that contributed from the optical telescope.

Logarithmic scale is then applied to the results of equation 8 in order to reduce the dynamic range of the image that observed by these techniques as shown in figures 10 to 13.

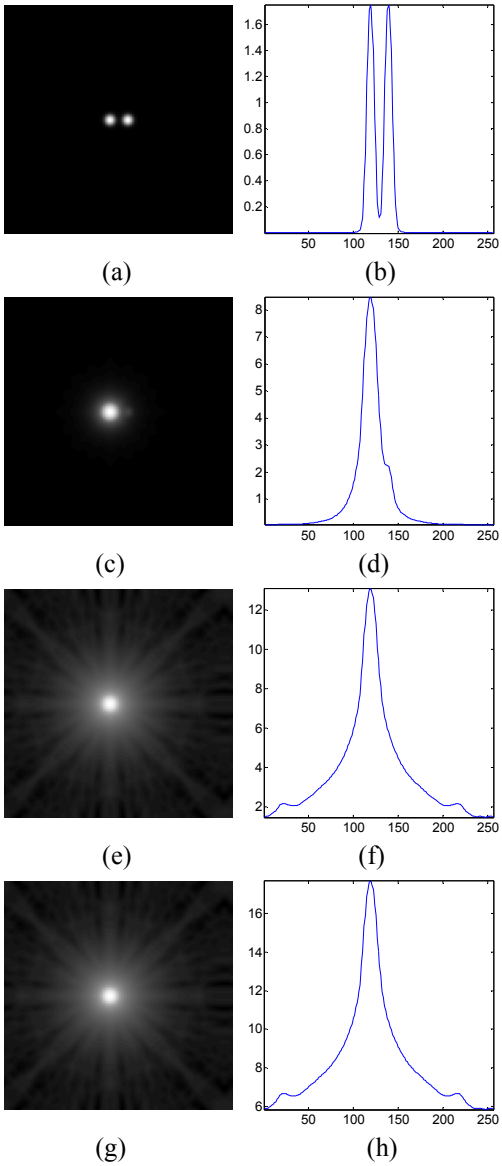

Figure 10- Logarithmic image of a binary system with a circle aperture using different CR, a-CR=1,b- Centeral plot through (a), c-CR=10^{-3}, d- Centeral plot through (c), e-CR=10^{-5}, f- Centeral plot through (e), g-CR=10^{-7} , and h- Centeral plot through (g).

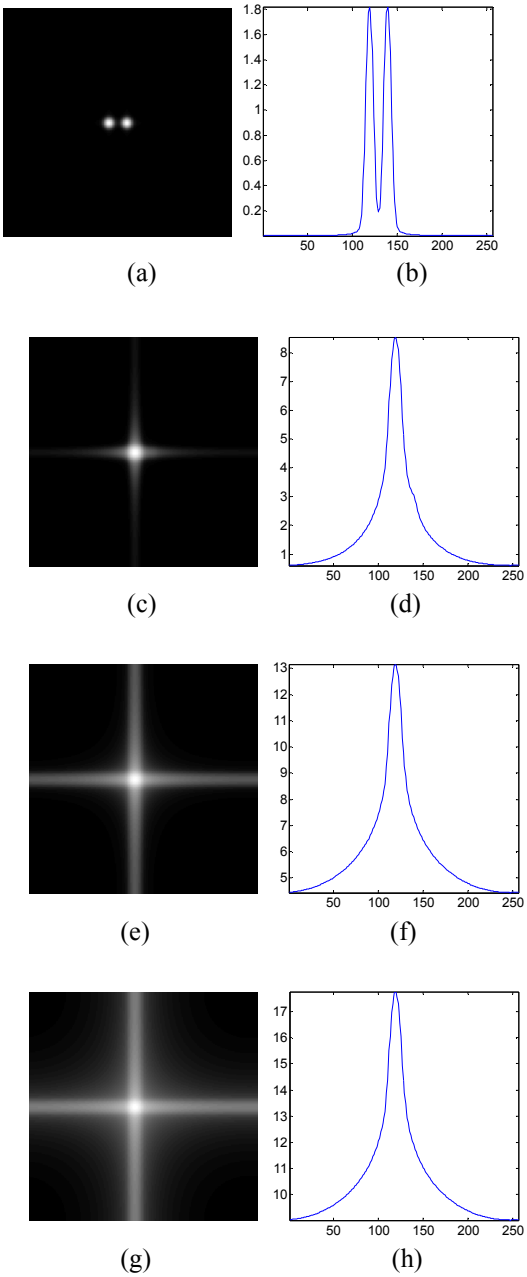

Figure 11-Logarthmic image of binary system with a square aperture using different CR, a-CR=1,b- Centeral plot through (a), c-CR=10^{-3}, d- Centeral plot through (c), e-CR=10^{-5}, f- Centeral plot through (e), g-CR=10^{-7}, and h- Centeral plot through (g).

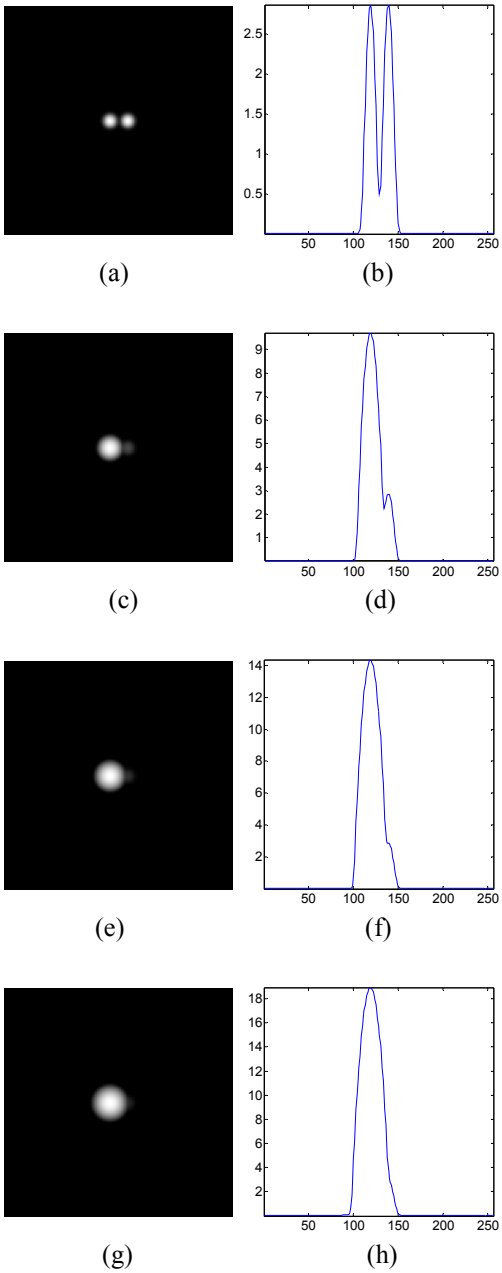

Figure 12-Logarthmic image of a binary system with a circular Gaussian shape aperture using different CR, a-CR=1, b- Centeral plot through (a), c-CR=10^{-3}, d- Centeral plot through (c), e-CR=10^{-5}, f- Centeral plot through (e), g-CR=10^{-7}, and h- Centeral plot through (g).

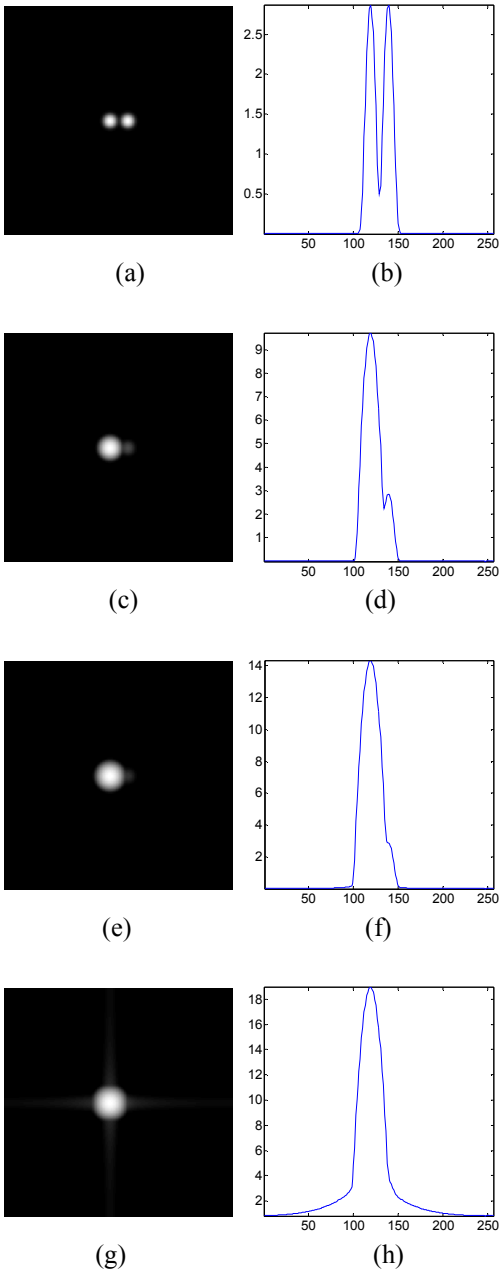

Figure 13- Logarthmic image of a binary system with a square Gaussian shape aperture using different CR, a-CR=1, b- Centeral plot through (a), c-CR=10^{-3}, d- Centeral plot through (c), e-CR=10^{-5}, f- Centeral plot through (e), g-CR=10^{-7}, and h- Centeral plot through (g).

The contour plots of figures (12 & 13) reveal the planet even at CR=1:10^{-7} as demonstrated below.

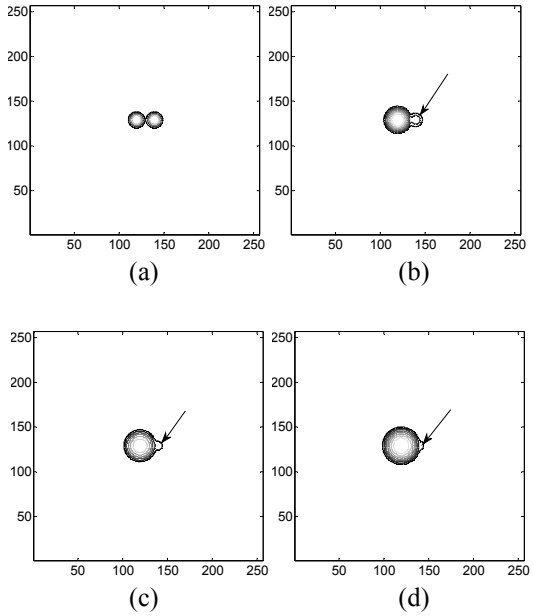

Figure 14- Contour plots of figure (12) a-CR=1, b-CR=10^{-3}, c-CR=10^{-5}, and d-CR=10^{-7}.

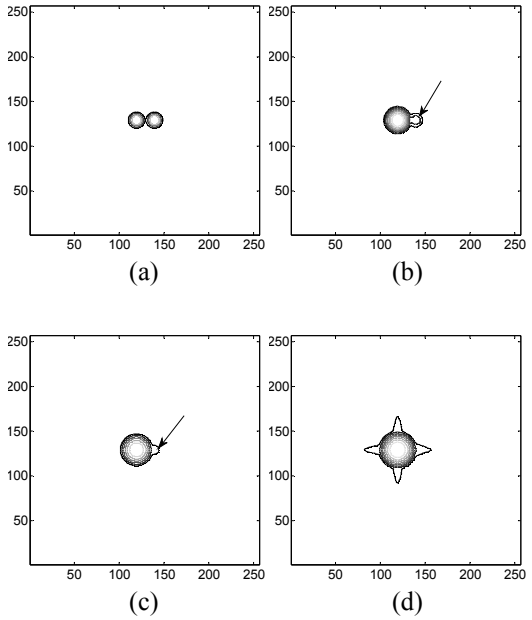

Figure 15- Contour plots of figure 13 a-CR=1, b-CR=10^{-3}, c-CR=10^{-5}, and d-CR=10^{-7}.

3. Conclusions

The important points that could be drawn from this study are summarized as follows:

1. The wings of the psf or the star are responsible for direct imaging of extrasolar planet. This attributed to the relative brightness of the star and the planet. The star makes the extrasolar planet lies beneath the wings of the psf and makes it impossible to observe any faint object nearby star.
2. The circular Gaussian shape aperture makes the wings of the psf or star to be decline to a limit that exceed 10^{-20} and this is a very promising result for direct observation of extrasolar planet.
3. The minimum value of the wing of the psf is proportional to σ of a circular and a square Gaussian shape apertures and obey third degree polynomial while the distance is inversely proportional with σ (see figures 8 & 9).
4. Contour plots reveal accurate indication of the existence of the planet even with CR=10^{-7} using a circular Gaussian shape aperture (see figure 14) while the square Gaussian shape aperture indicates the existence of extrasolar planet at CR=10^{-5} (see figure 15).

References:

1. Chakraborty, A. and Thompson, L. **2005**. 10^{-7} Contrast Ratio at 4.5 λ/D: New Results Obtained in Laboratory Experiments using Nano-Fabricated Coronagraph and Multi-Gaussian Shaped Pupil Mask. *Optics Express*, **13** (7),pp:2394-2402.
2. Yang, W. and Kostinski, A. **2004**. One-Sided Achromatic Phase Apodization for Imaging of Extrasolar Planets. The *Astrophysical Journal*, **605**,pp:892-901.
3. Nisenson, P. and Papaliolios, C. **2001**. Detection of Earth-Like Planets using Apodized Telescopes. *The Astrophysical Journal*, **548,**pp:L201-L205.
4. Galicher, R; Baudoz, P. and Baudrand, J. **2011**. Multi-Stage Four-Quadrant Phase Mask: Achromatic Coronagraph for Space-Based and Ground-Based Telescopes. *A & A*, **530**,pp:A43.
5. Spergel, D. **2001**. A New Pupil for Detecting Extrasolar Planets. *Bulletin of the American Astronomical Society*.**33**,pp:1431-1445.
6. Martinez, P; Dorrer, C; Carpentier, E; Kasper, M; Boccaletti, A; Dohlen, K. and Yaistkova, N. **2009**. Design, Analysis, and Testing of a Microdot Apodizer for the Apodized Pupil Lyot Conogagraph. *A & A*, **495**,pp:363-370.
7. Enya, K, Kotani,T, Haze, K, Aono, A, Nakagawa, T, Matsuhara, H, Kataza, H, Wada, T Kawada, M, Fujiwara, K, Mita, M, Takeuchi, S, Komatsu, K, Sakai, S, Uchida, H, Mitani, S, Yamawaki, T, Miyata, T,Sako, S, Nakamura, T, Asano, K, Yamashita, T, Narita, N, Matsuo, T, Tamura, M, Nishikawa, J, Kokubo, E, Hayano, Y, Oya, S, Fukagawa, M, Shibai, H, Baba, N, Murakami, N, Itoh, Y, Honda, M, Okamoto, B, Ida, S, Takami, M, Abe, L, Guyon, O, Bierden, P. and Yamamuro T. **2011**. The SPICA Coronagraphic Instrument (SCI) for the Study of Exoplanets. *Advances in Space Research*, **48**,pp:323-333.
8. Postman,M, Traub, W, Krist, J,Stapelfeldt, K, Browen, R, Oegerle, W, Lo, A, Clapin, M, Soummer, R, Wiseman, J. and Mountain, M. **2010**. Advanced Technology Large-Aperture Space Telescope (ATLAST): Characterizing Habitable Worlds. Proceeding of the ASP Conference Series. Barcelona, Spain,pp: 14-19 Sep.
9. Soummer, R. **2005**. Apodized Pupil Lyot Coronagraphs for Arbitrary Telescope Apertures. *The Astrophysical Journal*, **618** ,pp:L161-L164.
10. Kalas, P;Graham, J, Chiang, E, Fitzgerald, M, Clampin, M, Kite, Stapelfeldt, K, and Krist, J. **2008**. Optical Images of an Exosolar Planet 25 Light Years from Earth. *Science*, **322**,pp:1345-1370.

11. Mallbet, F; Yu, J. and Shao, M. **1995**. High Dynamic Range Imaging using a Deformable Mirror for Space Corongraphy. *PASP*, **107**,pp:386-398.
12. Martinache, F; Guyon, O; Pluzhnik, E. and Galicher,R. **2006**. Exoplanet Imaging with a Phase-Induced Amplitude Apodization Coronograph II. Performance. *The Astrophysical Journal*, **639**,pp:1129-1137.
13. Miller, V.R. **2009**. A Search for Transiting Extrasolar Planets and Variable Stars in the Galatic Plane. Ph.D. Thesis, Department of Physics and Astronomy, University of Canterbury, PP.10-11.
14. Evans, J.W. **2006**. High Contrast Imaging using Adaptive Optics for Extrasolar Planet Detection. Ph.D. Thesis. Engineering – Applied Science, University of California, PP.56-58.
15. Aime, C; Soummer, R. and Ferrari, A. **2002**. Total Coronagraphic Extinction of Rectangular Apertures using Linear Prolate Apodizations. *A & A*, **389**,pp:334-344.
16. Creep, J.R.**2008**. High- Contrast Imaging with a Band-Limited Coronographic Mask. Ph.D. Thesis. Physics Graduate School, University of Florida. PP.75-77.
17. Mohammed, A.T. **2007**. Limits of the Efficiency of Imaging with Obstructing Apertures. *SQU*:*Sultan Qaboos University Journal for Science*, **12**(1),pp:67-74.